ACCURATE ENERGY MEASUREMENTS ON A 50 MeV PROTON LINEAR ACCELERATOR*

K. Batchelor, A. Carne, J. M. Dickson, D. J. Warner
Rutherford High Energy Laboratory, England

Energy measurements have been carried out on the three accelerating sections of the Rutherford High Energy Laboratory Proton Linear Accelerator i. e. at 10 MeV, 30 MeV and 50 MeV. The measurement utilises a cambination of accurate redio frequency deflection of the input beam to the accelerator, thus increasing the proton burst spacing, and precise timing of the flight time of individual bursts over an accurately known distance at the end of the accelerator.

1. OUTLINE OF THE TIME OF FLIGHT METHOD OF ENERGY MEASUREMENT

a. General principles

Under normal operating conditions the P. L. A. accelerates protons to 10, 30 and 50 MeV and gives 200 μs long pulses at a rate of 50 per second. The phase bunching action of the accelerating field at 202.5 MHz produces a fine structure of proton bursts less than 0.5 ns long separated by 4.94 ns. By phased radio frequency deflection of the 520 keV proton beam from the injector across a slit, the burst spacing ray be increased (see Fig. 1). In particular by RF deflection at 11.25 MHz, bursts of protons pass through the slit every 44.44 ns. However, since the protons pass through axial electric fields on enternig and leaving the deflector plates velocity modulation of the beam occurs, as a result it can be shown that

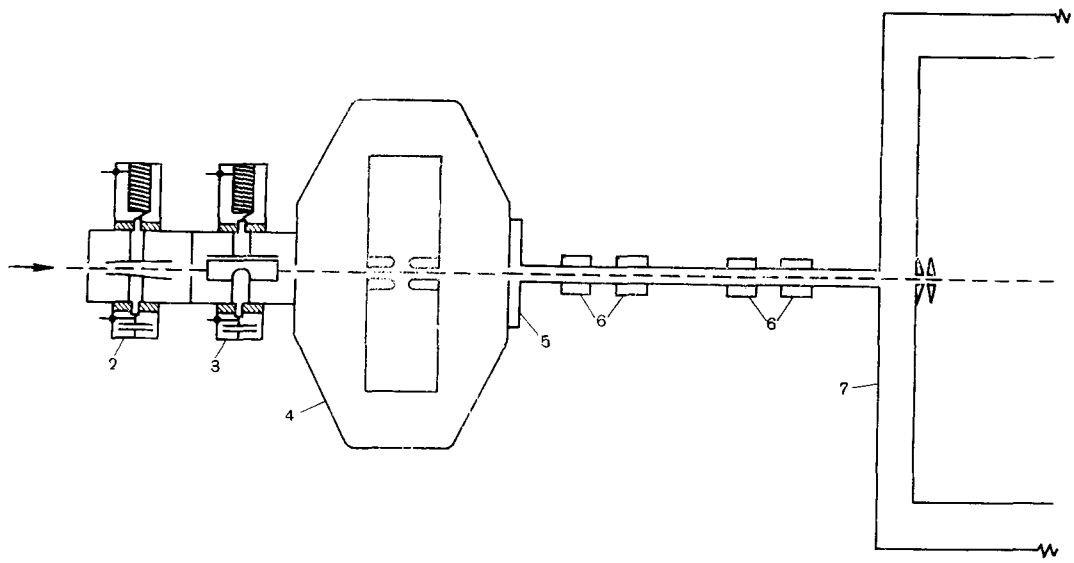

Fig. 1. Arrangement in low energy drift space:
1 —520 keV protons; *2* — deflector A; *3* — deflector B; *4* — buncher; *5* — defining aperture; *6* — quadrupoles; *7* — tank 1.

The effect of various machine parameters on the output beam energies has been investigated, the main parameters used being radio frequency field amplitude, inter tank phase and field tilt. Computer programmes have been written, using step by step integration of the cavity fields, which enable one to compare the above results with theory.

* The report was not read.

with a deflection voltage of 10 kV peak, if one proton pulse arrives at the first accelerating gap in Tank 1 at the most favourable time for acceptance, the following pulse will arrive at the least favourable time and will not be accelerated. In this way the burst spacing is increased to 88.89 ns.

The RF deflector voltage also provides, after suitable shaping, a series of accurate timing pulses spaced by 88.89 ns, which are accurately phased to the proton bursts from the machine.

The time difference between the arrival of a proton at a scintillation counter and the next timing pulse can then be measured using a time to amplitude converter (time sorter). If now the counter is moved back a distance corresponding to a flight time for the proton of 88.89 ns or multiple thereof, then the time difference measured by the time sorter will be the same in both cases. In actual practice a fixed flight path approximately equivalent to this flight time is used and the (small), difference between the flight time and the burst spacing measured. Most of the results reported were taken using a flight path of about 26 m corresponding to flight times of 622 ns ($\sim 7 \times 88.89$ ns) for 10 MeV, 356 ns ($\sim 4 \times 88.89$ ns) for 30 MeV and 267 ns ($\sim 3 \times 88.89$ ns) for 50 MeV protons.

In order to eliminate drifts between spectra taken with the counter in the first position and then in the second position, a second counter is used to provide reference time spectra. The experimental arrangement is shown in Fig. 2.

b. The timing system

For reasons described in an earlier report on the Time of Flight Measurement [2] the protons are scattered elastically through 30° by a 0.0002″ thick Aluminium foil into a scintillator having a solid angle of 2×10^{-3} sterad. The overall sampling efficiency is 1 in 10^8.

The scattered protons when stopped in a type NE102 plastic scintillator viewed by a 56 AVP fast multiplier tube, provide start pulses for an A. E. R. E. Type 2011A nanosecond time to amplitude converter [3]. Stop pulses for this «time sorter» are derived from the deflector plates as described earlier. Pulses from the photomultipliers 13th dynode are used in a «slow side» disoriminator which gates the output of the «time sorter» only for pulses corresponding to elastically scattered protons. Initially the discriminator is set by reference to the pulse height spectrum from the detector «slow side». With the deflector powered in the mode required [4] i. e. 88.89 ns. burst spacing, the beam current is adjusted so that the count rate of pulses into the «kick sorter» is less than 50 per second. The time sorter range, kick sorter gain and back bias and stop-pulse

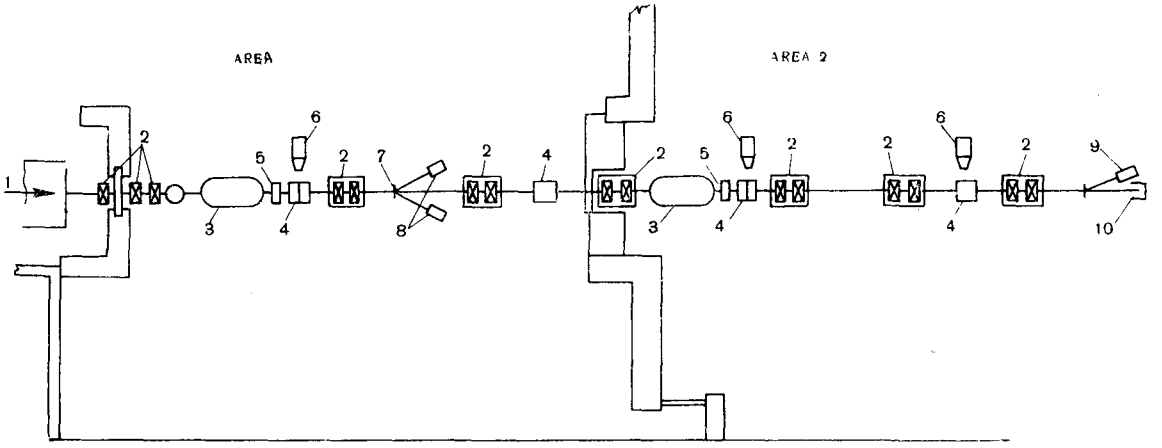

Fig. 2. Experimental layout for energy measurements:

1 — beam from plasmatron; *2* — quadrupoles; *3* — bending magnet; *4* — flip in scintillator; *5* — vacuum valve; *6* — TV camera; *7* — scattering foil and double «Y» piece; *8* — scintillation counters; *9* — scintillation counter (moved to the area from area 1 for comparison); *10* — faraday cup.

delay are adjusted so that the required features of the spectrum are displayed.

Fig. 3 is a schematic diagram of the electronic apparatus used.

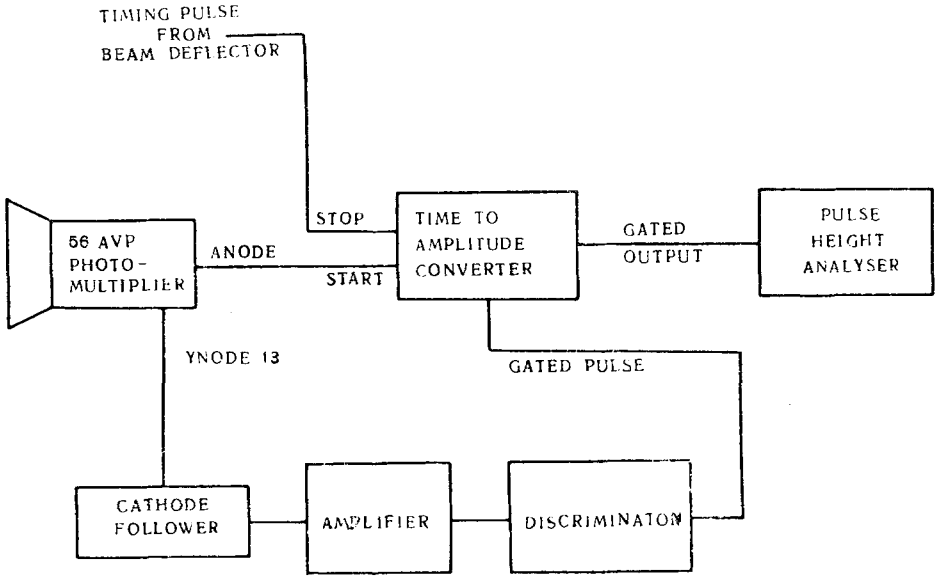

Fig. 3. Block diagram of electronics.

c. Measurement of energy and energy shifts

Any process which causes the arrival of a proton at a detector to vary in time relative to the deflector excitation phase shows up as a time shift in the time spectrum. A change in energy ΔE from a reference kinetic energy E causes a change in flight time between the end of the last accelerating tank and the detector.

$$\frac{\Delta t}{t} = -\frac{1}{2}\frac{\Delta E}{E}\left\{1+\frac{3E}{2E_0}+\right.$$
$$\left.+\frac{1}{2}\left(\frac{E}{E_0}\right)^2\right\}^{-1} \simeq -\frac{1}{2}\frac{\Delta E}{E} \qquad \text{(A)}$$

E_0 is the rest mass energy of the proton at 30 MeV the approximate form is good to 5%.

Any flight time variations between the deflectors and the end of the accelerating section must also be taken into account. The flight time through each powered tank varies from an exact number of radio-frequency cycles by an amount dependent on the amplitude and wavelength of the phase oscillations. With the flight paths used, for 10 MeV and 30 MeV protone, the correction to the energy shift given by Eqn. A, for protons observed at the scatterer nearest to the end of the accelerator, is less than 10%. For 50 MeV protons the correction (with the short flight path available to this position of about 9m) maybe of the same order as the time variation due to energy shift so that the interpretation of energy shift results is more difficult.

To make an accurate energy measurement several spectra must be taken with one counter in each of the two scatter positions whilst the other remains in the same position at the first scatter position. Alternate spectra are taken on this fixed counter for reference purposes. Let us designate the counters *C1* and *C2* and the positions *A1* and *A2*. Then counter *C1* remains in position *A1*, whereas counter *C2* moves from *A1* to *A2*.

The time of flight for the proton beam is given by

$$t = n \times 88.888 - \{C2\,(A2) - C1\,(A1)\} +$$
$$+ \{C2\,(A1) - C1\,(A1)\}\,ns,$$

where $n = 7$, 4 or 3 for 10, 30 or 50 MeV protons respectively and where $\{C2\ (A2) - C1\ (A2)\}$ is the time difference between spectra from counter *C2* in position *A2* and counter *C1* in position *A1*. Simitarly *C2* (*A1*) — *C1* (*A1*)

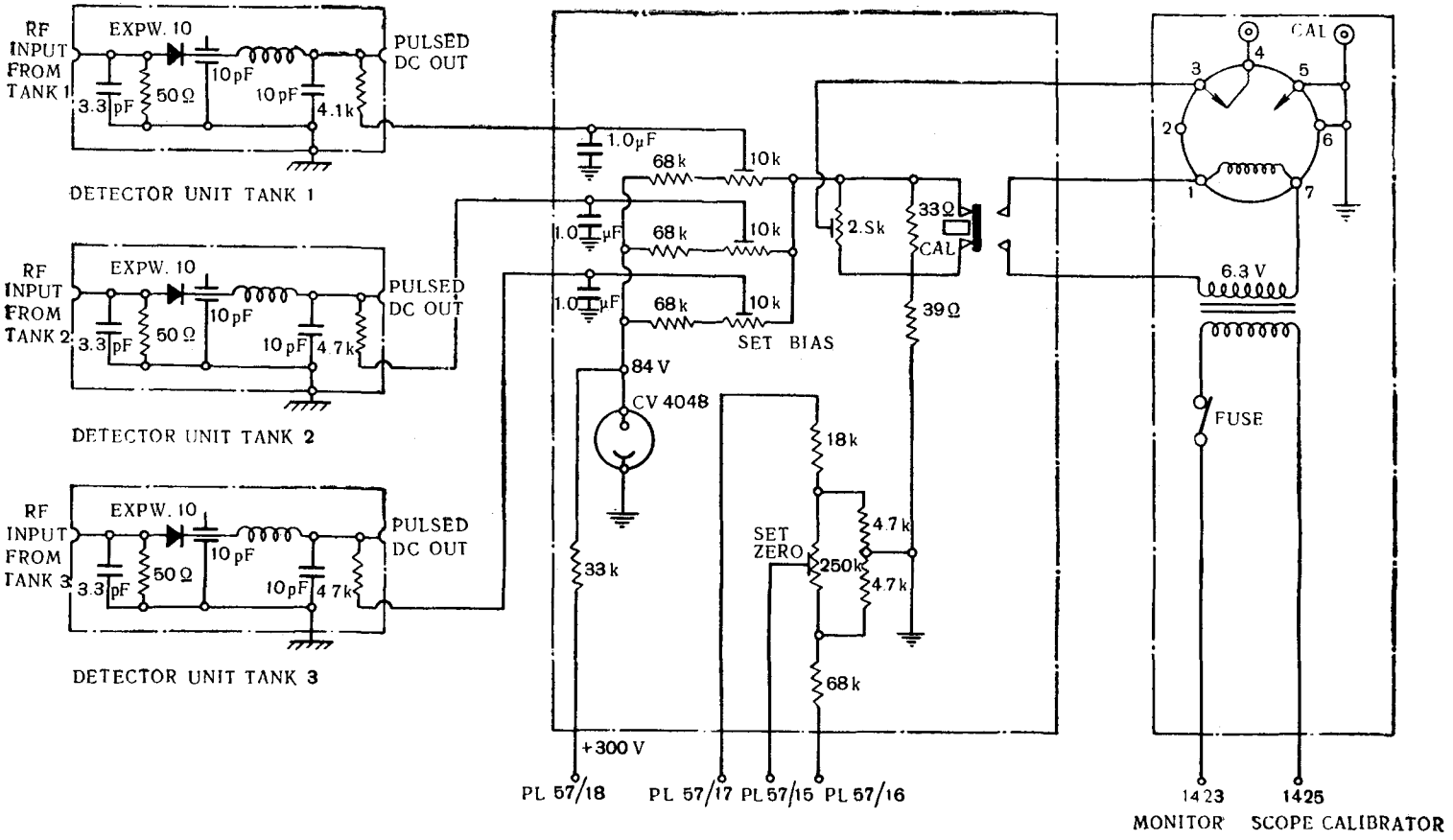

Fig 4. Accurate RF field monitor.

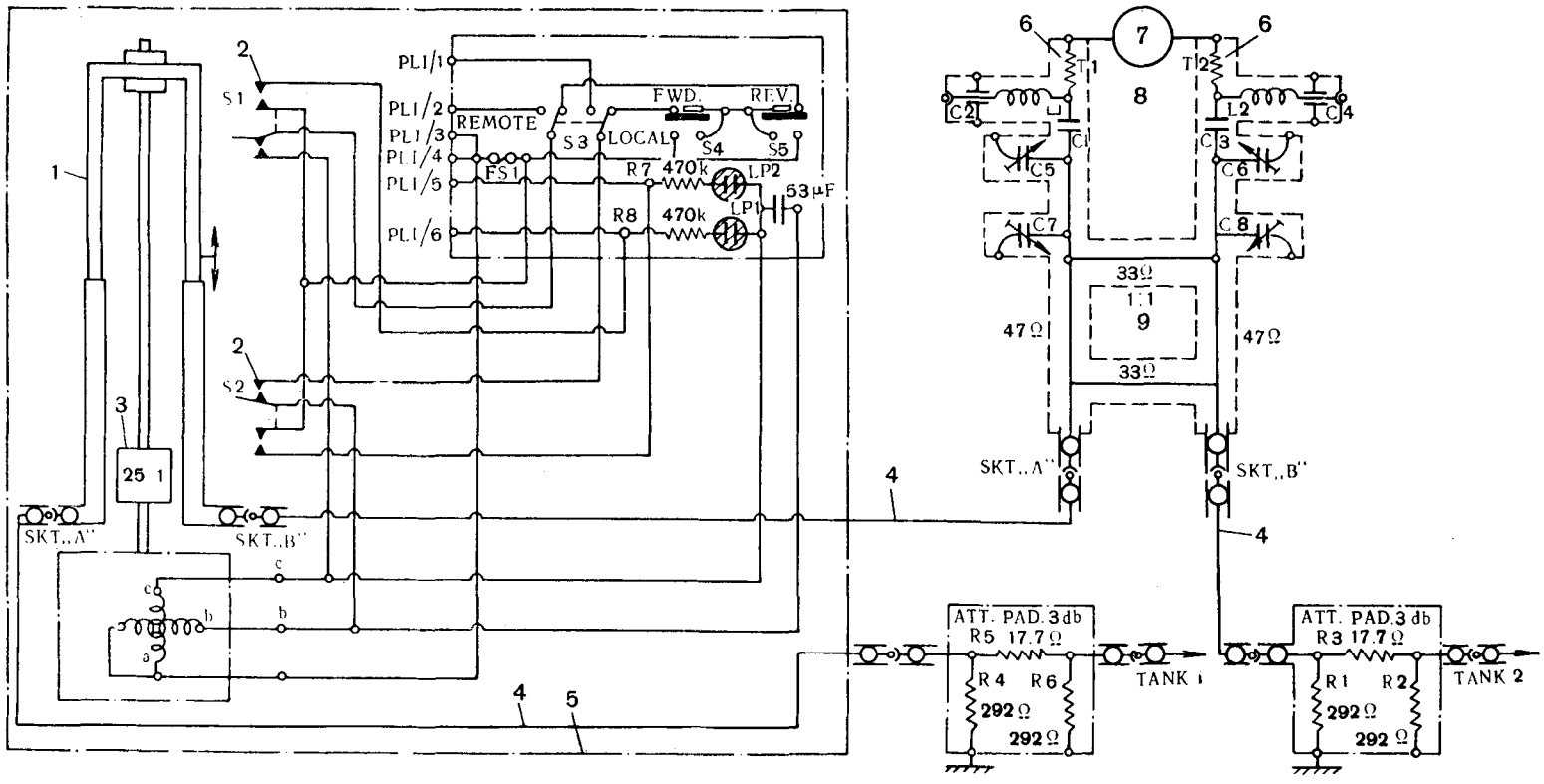

Fig. 5. Phase bridge units for inter-tank phasing systems. Key:

PL1/1 line lengthener drive motor (fwd.); PL1/2 line lengthener drive motor (rev.); PL1/3 230 V mains neutral; PL1/4 230 V mains line; PL1/5 motor limit switch (rev.); PL1/6 motor limit switch (fwd.); *1* — dielectric loaded line lengthener; *2* — limit switch S1; *3* — gear box; *4* — 50Ω coaxial cable UR43; *5* — line lengthener; *6* — thermocouple CV357; *7* — phase bridge meter; *8* — coaxially mounted thermocouples; *9* — phase bridge.

is the time difference between spectra from counter *C2* in position *A1* and counter *C1* in position *A1*.

In order to determine these time differences the centroid of each spectrum is calculated using a computer program which also determines the significance of any high or low energy «tails» observed on the spectrum.

When several repeated runs are taken it is possible to determine the quantity $\{C2\ (A2) - C1\ (A1)\}\{-\}\{C2\ (A1) - C1\ (A1)\}$ to within an error of $\pm 0{,}1$ ns.

2. MONITORING

a. RF Monitoring

After some of the early, measurements had been carried out it became evident that reliable radio frequency field level metering and inter-tank phase monitoring were essential in order to obtain repeatable results from subsequent observations. At this time no inter-tank phase monitor was available and the best indication of RF field level was the forward power reflectometer in the feed line to each tank, which was accurate to a few per cent if undisturbed.

The early results indicated that field level accuracy of the order of 0.1% was desirable, whereas the inter tank phase should be controlled to $\pm 1°$. Accordingly a circuit using a semiconductor diode backed off by an accurate dc voltage was developed (Fig 4) for RF level monitoring and phase bridges using thermocouple detectors feeding a galvonometer (Fig. 5) were used to measure inter-tank phase. The phase meter was calibrated against an adjustable phase shifter which was introduced into one arm of the bridge.

b. Beam Monitoring

The Faraday cup monitors between tanks were used. The threshold energies of the 10, 30 and 50 MeV cups can be made 9.5, 29, and 48.5 MeV respectively, thus allowing them to record only «stably» accelerated protons.

A further Faraday cup at the end of the beam pipe (Fig. 2) was used for continuous beam monitoring during the experiment. A count rate meter on the discriminator dynode pulses was also used for normalisation of the spectra taken during the energy measurements.

3. EXPERIMENTAL RESULTS

On the P. L. A. several parameters vary the output beam energy of each section. These parameters are (1) the input energy, (2) the input phase, (3) the field tilt, (4) the RF field level. Some measurements have been made for each of these on some or all three tanks. In addition, the output energies of the three accelerating sections under the normal operating conditions were measured.

a. Results for Tank 1 (10 MeV)

1) Output energy as a function of input energy for various RF field levels in Tank 1

Two sets of results have been taken for injection energies of 500 and 520 keV. The resulting spectra are plotted in Figs. 6 and 7. These spectra show the familiar peaks [5] attributed

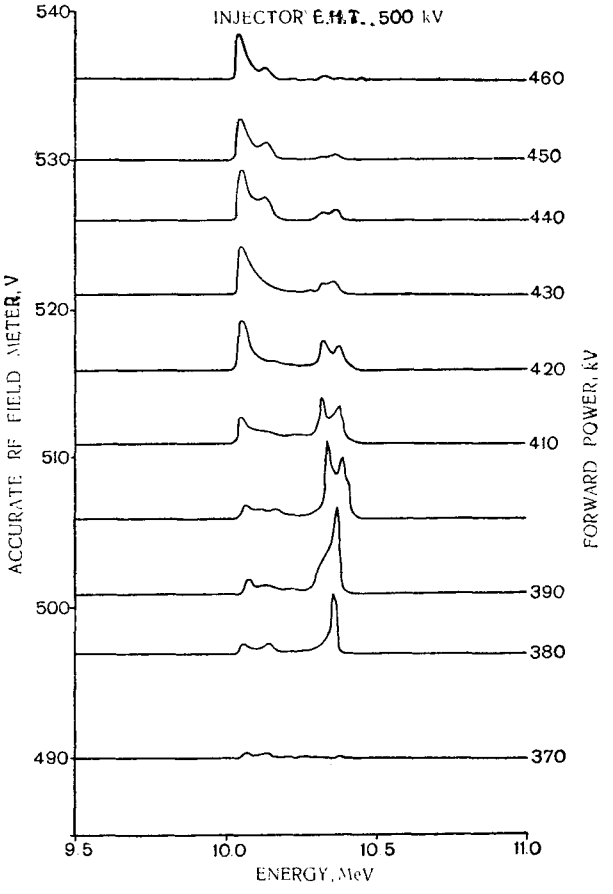

Fig. 6. 10 MeV energy vs. RF level for injection at 500 keV.

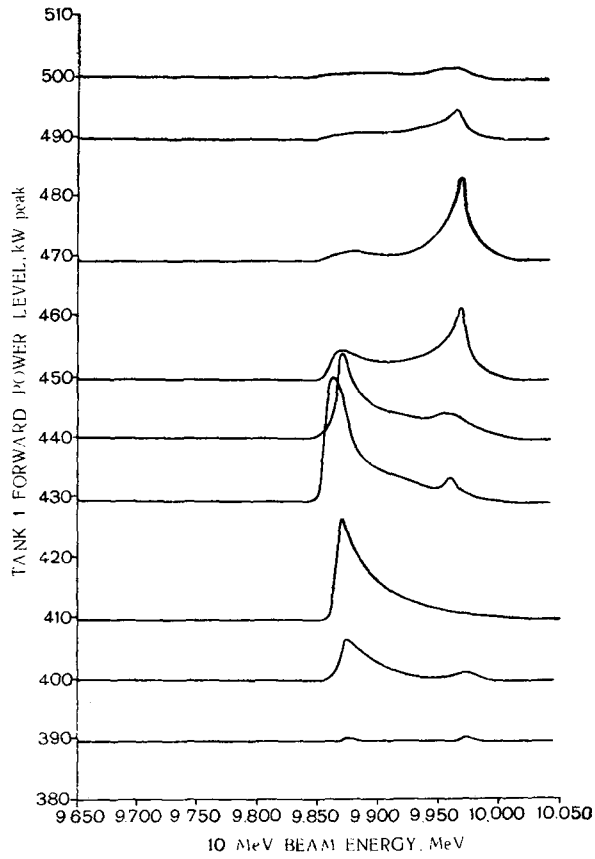

Fig. 7. 10 MeV energy vs. RF level for injection at 520 keV.

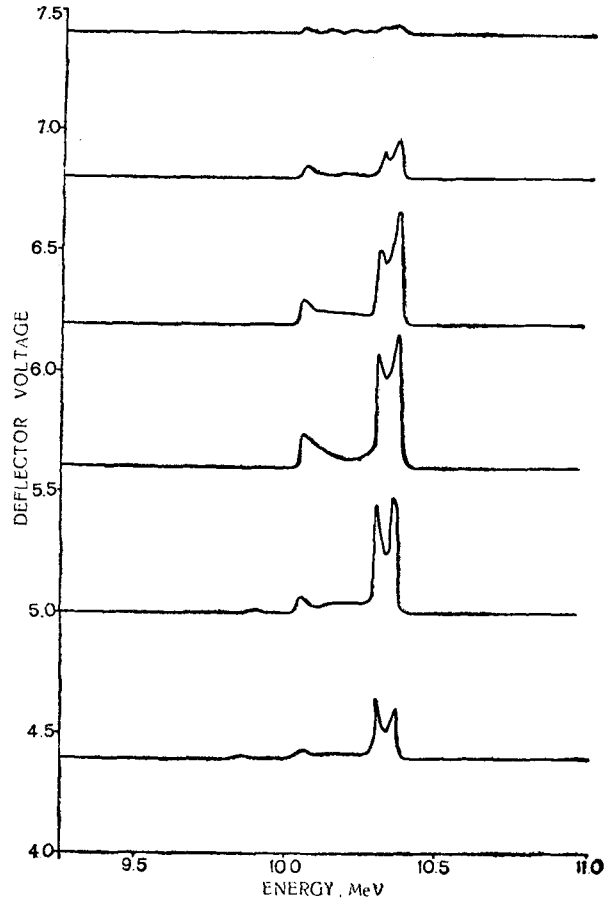

Fig. 8. 10 MeV energy vs. input phase.

to «filamentation» caused by excursions into the non-linear regions of the phase motion. The curves show a shift of the mean energy as the RF level is increased the shift being in opposite directions for the two injection energies considered. Also the mean energy is higher for the lower injection energy than it is for the higher. The area of each output spectrum is proportional to the average beam current obtained at that setting.

2) Output energy as a function of input phase for various RF field levels

Here we have only one set of spectra for an injection energy of 500 keV and one RF level (400 kW forward reflectometer reading) in Tank 1. The relatively large phase width of the injected beam (~70°) makes interpretation of the results difficult but it would seem that at this RF field level in Tank 1 there is no change of output energy with change of input phase i. e. there is an even number of half wavelengths of phase oscillation along the tank. The spectra obtained are plotted in Fig 8.

3) Output energy as a function of field tilt for various RF field levels

The results obtained have no absolute energy scale due to the fact that only one counter was used for this experiment. The energy shifts produced by tilting the field are shown in Fig. 9. The actual shift in mean energy is small but the power level in the cavity has to be increased considerably as the field at the input end is reduced, thus reducing the phase acceptance.

4) Normal operating conditions

Two energy measurements have been made with Tank 1 at its normal operating level but

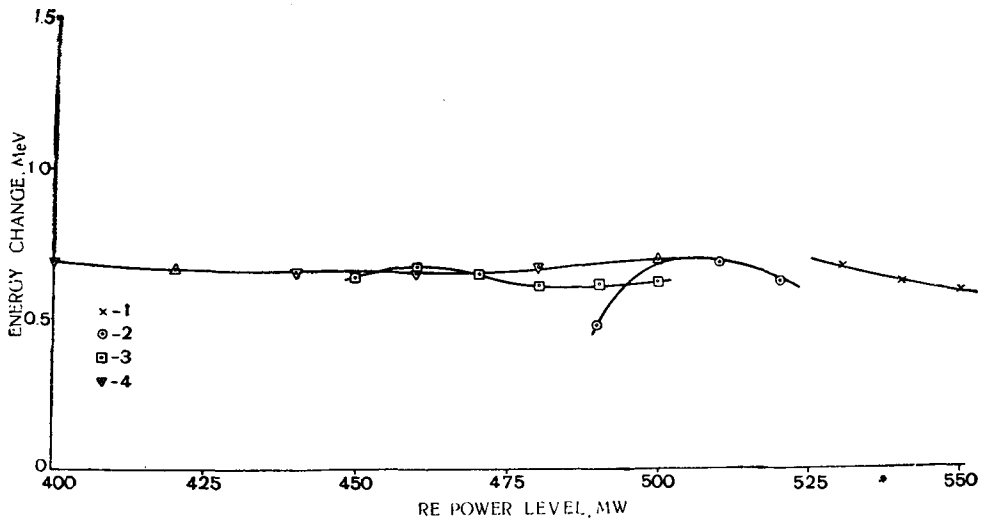

Fig. 9. 10 MeV energy shift vs. RF field level for various field tilts: *1* — tilt $75-25 \frac{\text{input end field}}{\text{output end field}} = 0.86$; *2* — tilt $50-50 \frac{\text{input end field}}{\text{output end field}} = 1.0$; *3* — tilt $25-75 \frac{\text{input end field}}{\text{output end field}} = 1.12$; *4* — tilt $0-100 \frac{\text{input end field}}{\text{output end field}} = 1.25$.

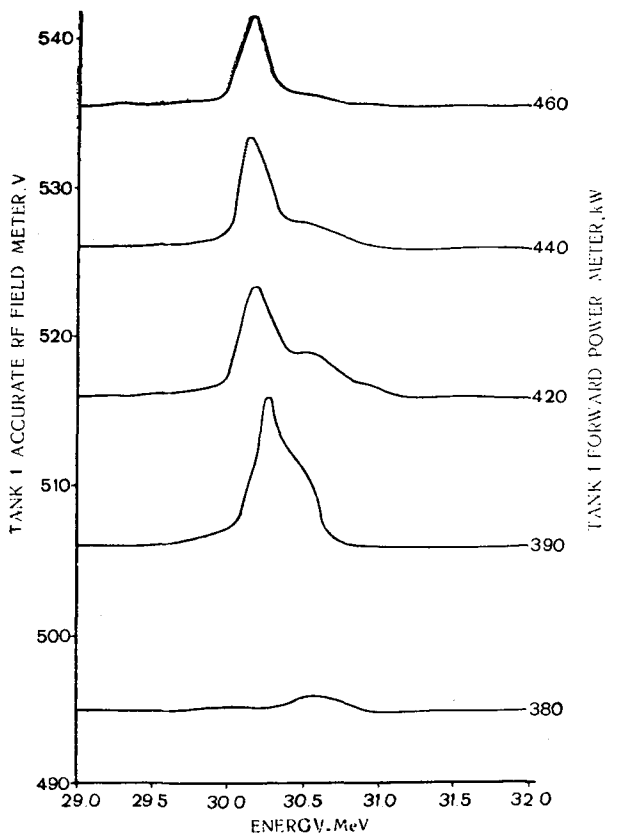

Fig. 10. 30 MeV energy vs. input energy for injection at 500 keV into tank 1. Injector E.H.T. = 500 kV. Tank 2 accurate RF = 565. Forward power = 1.02 MW.

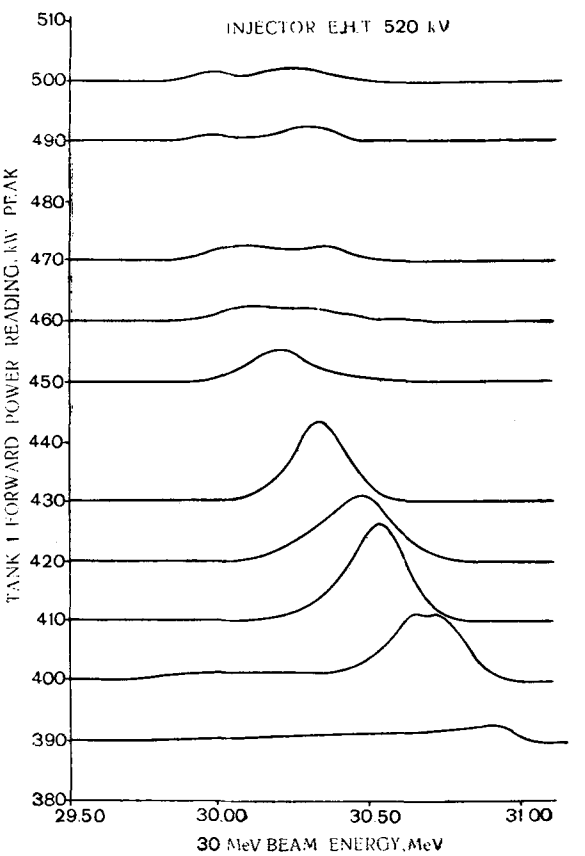

Fig. 11. 30 MeV beam energy and current as a function of input energy for injection at 520 keV into tank 1. Injector E.H.T. = 520 kW.

with two different injection energies. The results were as follows: a) injection energy 500 keV, mean output energy (10.215±0.025) MeV, b) injection energy 520 keV, mean output energy (9.915±0.015) MeV.

Computational results for Tank 1 are not yet available but will be included in a full report to be published. The errors quoted on the output energy are the standard deviations of the experimental errors.

b. Results for Tank 2 (30 MeV)

1) Output energy as a function of input energy

The results obtained are shown in Figs. 10 and 11. The spectra are plotted for various RF field levels in Tank 1, the actual input spectra at these levels being those plotted in Figs. 6 and 7. The large energy shifts exhibited can be explained in terms of a wide and varying output phase spread from Tank 1. This wide phase spread results from the large field tilt, of the order 25% and to end, of the Tank 1 axial field.

2) Output energy as a function of input phase for various RF field levels

The results obtained for a mean injection energy of 9.915 MeV are plotted in Fig. 12, and

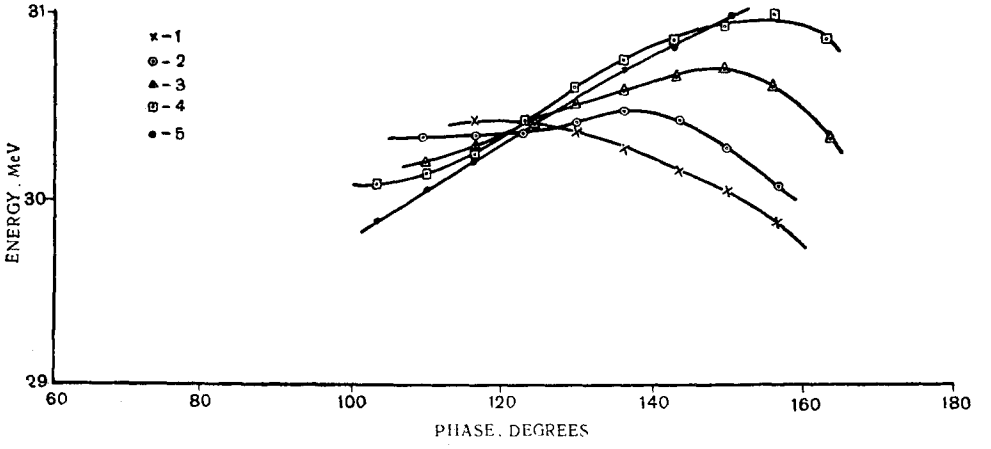

Fig. 12. 30 MeV energy vs. input phase-experimental. Tilt 60—40. Injector energy 9.91 MeV. Centroids used for energy scale. Arbitary zero on phase scale:
1 — RF level = 33.0; *2* — RF level = 34.0; *3* — RF level = 35.0; *4* — RF level = 36.0; *5* — RF level = 37.0.

may be compared with the results from the computer programme in Fig. 13. There is some difficulty in defining RF field levels for comparison between theory and practice. The acceptance phase plots show a wide input phase acceptance due to the large tilt on the axial field which is high at the input end, by about 20% over the average field. Many of the protons reaching the final energy would be lost completely if the tank were longer thus allowing a greater number of phase oscillations.

3) Normal operating conditions

Two measurements have been made for injection energies of 9.91 and 10.215 MeV the RF power levels in Tank 2 being 1 MW and 1.02 MW respectively and injection at the stable phase angle as defined by an «acceptance phase» plot. For injection at 9.915 MeV, output energy = 30.48±0.04 MeV. For injection at 10.215 MeV, output energy = 30.40±0.01 MeV. The field tilt was 60—40 for both measurements.

c. Results for Tank 3

No specific data has been taken for output energy as a function of input energy or input phase and very little computational work has been carried out for this tank.

1) Output energy as a function of field tilt

Two sets of results have been obtained and are plotted in Fig. 14.

2) Normal operating conditions

Three measurements have been made all for injection at the stable phase angle as defined by an «acceptance phase» plot. The results

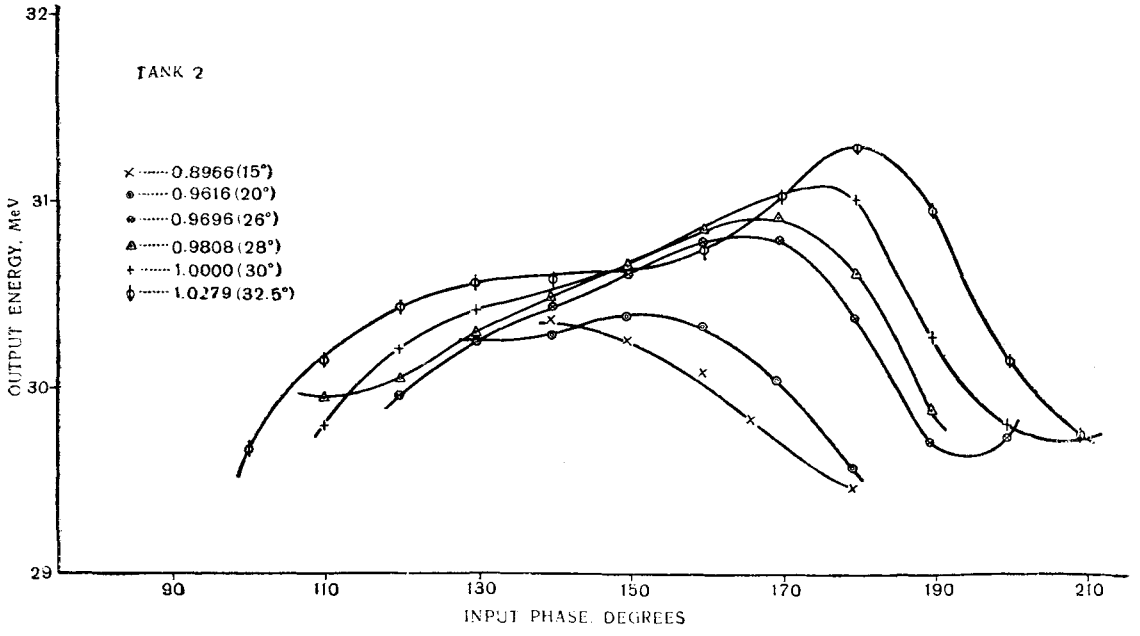

Fig. 13. 30 MeV energy vs. input phase-computational. Axial motion. Practical tilts 60—40 $\frac{\text{input field}}{\text{output field}} =$ $= 1.05$. Input energy 9.910 MeV. Phase angles in degrees defines at the centre of the tank.

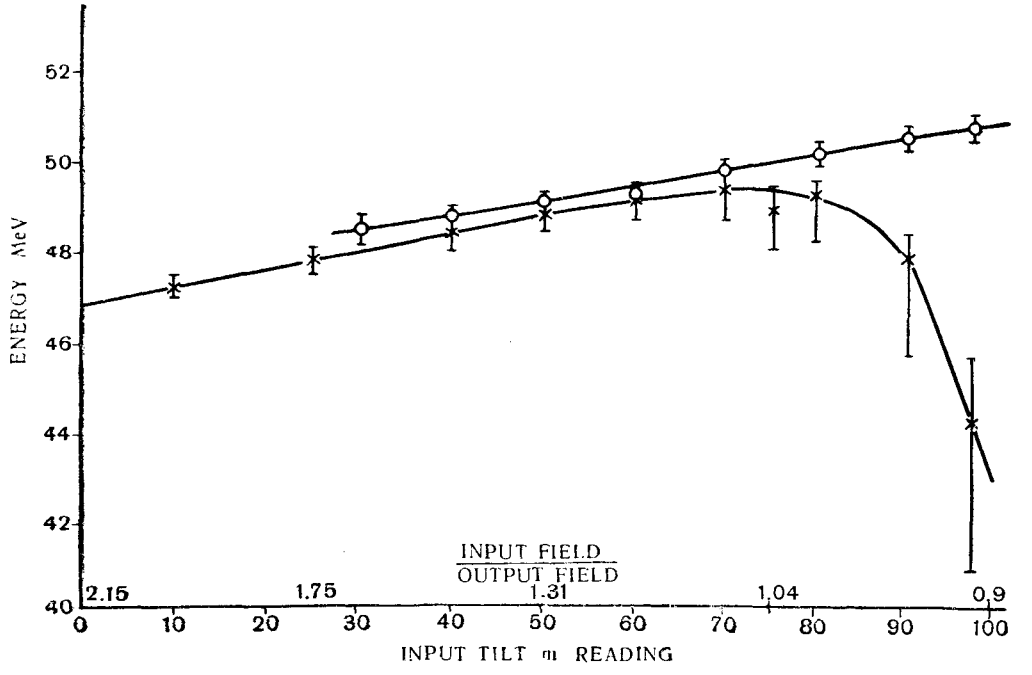

Fig. 14. 50 MeV energy vs. field tilt. Energy vs. input tilt (symmetrical tilts, $\Phi sh =$ $=56$). The bars show the full width at half height of the spectra.

were as follows:

Injection Energy	Tilt	Power	Output Energy
30.48 MeV	70/30	1.20 MW	49.54±0.04 MeV
30.40 MeV	75/25	1.28 MW	49.02±0.05 MeV
30.40 MeV	75/25	1.35 MW	50.02±0.05 MeV

4. DISCUSSION

The accurate energy measurements can be seen to be accurate to better than 0.2% for all energies, indicating the usefulness of the time of flight method for this measurement. In setting up a high-energy linac, 100 MeV energy or greater, an energy measurement, for each accelerating section, of this order of accuracy may be necessary. The computational results obtained so far show reasonable agreement with the experimental ones. A more precise method of comparison will be made in the future. It is clear that the optimisation of beam current method adopted for setting up an accelerator is useful only for a few accelerating cavities and even then does not produce the best output beam in terms of energy and phase spread. It is also possible to make some estimats of the RF field amplitude and phase tolerances required to maintain a stable output beam energy.

ACKNOWLEDGEMENTS

We wish to thank Dr. C. Batty for loan of much of the electronic apparatus, A. P. Banford, R. Worsham, E. M. Mott, C. A. Baker, P. Mackay and D. Carpenter for assistance during experimental runs and D. Carpenter, L. Goodall and J. Sherwood for assistance in the analysis and presentation of the results. Thanks are also due to the machine technicians for operating the machine. The program for the study of axial motion in Tanks 2 and 3 is based on that in ref. [1] by Dr. R. Taylor of the Rutherford Laboratory, to whom thanks are due.

REFERENCES

1. Taylor R. Acceptance of axially and radially oscillating particles in the Linac Injector for the 7 GeV Harwell Proton Synchrotron (Nimrod). AERE, R3013.
2. Batty C. J., Warner D. J. An accurate determination of the P. L. A. beam energy by a time of flight method. NIRL/R/9.
3. Wells F. H., Barlow A. K. Nanosecond time to amplitude convertor Type 2011A. AERE, R2903.
4. PLA Progress Report, 1961.
5. West N. D. Investigation of energy spread in the beam from the Nimrod Injector Linac. NIRL/M/46, Febr. 1963.